

Comparison of Adaptive Filtering in Time-, Transform- and Frequency-Domain: An Electrogastrographic Study

JIAN DE Z. CHEN and ZHIYUE LIN

Health Science Center, University of Virginia, Charlottesville, VA

Abstract—Adaptive cancellation of motion artifacts in the electrogastrogram (EGG) is presented in this paper. The EGG is a surface measurement of gastric electrical activity. Like other noninvasive electrophysiological measurements, the EGG contains motion artifacts. A number of papers have been published on the adaptive cancellation of motion artifacts or interferences in biomedical signals. Adaptive filtering was performed in time domain in almost all of the previous publications. In this paper, however, three different sorts of adaptive filters were investigated and their efficiencies in cancellation of motion artifacts were compared with each other. These include time-domain, transform-domain, and frequency-domain adaptive filters. A series of simulations were conducted to investigate the performance of these adaptive filters in cancellation of respiratory and motion artifacts. The results show that the frequency-domain adaptive filter has superior performance over the time- and transform-domain adaptive filters in the cancellation of stationary respiratory artifacts in the EGG. Although results focus on the EGG, this paper provides useful information for adaptive filtering of other biomedical signals.

Keywords—Adaptive filter, Signal processing, Noise cancellation, Electrogastrogram, Motion artifacts.

INTRODUCTION

Electrogastrogram (EGG) is a surface measurement of electrical activity of the stomach. It can be acquired by placing silver-silver chloride electrodes on the abdomen over the stomach (5). The electrical activity of the stomach is mainly composed of rhythmic slow waves. The frequency of the gastric slow wave in humans is about 3 cycles/min (cpm) in normal situations and can be as high as 9 cpm in abnormal situations. Previous studies have shown that the EGG reliably reveals the slow wave of the stomach (12).

While the noninvasive EGG is attractive, it has problems like other surface electrophysiological measure-

ments. The main drawback of the EGG is the poor quality of the recording. It contains heavy noise and interferences, such as electrocardiogram (ECG), respiratory, and motion artifacts. Respiratory and motion artifacts are very annoying in the EGG because: (a) they are usually strong and may completely obscure the electrical signal of the stomach; and (b) their frequencies overlap with or are close to that of the gastric electrical activity. Although the frequency of respiration ranges from 12 cpm to 24 cpm, which is higher than the gastric signal frequency, the use of conventional low-pass digital filtering may not be adequate. Since the electrical signal of the stomach is not sinusoidal, conventional digital filtering may distort waveforms of the gastric signal by filtering out harmonics of the fundamental frequency of the gastric signal. The motion artifact has a broad-band spectrum and its frequency is within the whole range of the recording frequency. Therefore, it cannot be eliminated by using conventional digital filtering without affecting the gastric signal.

Adaptive noise cancellation technique has been shown to be efficient in solving the problem where the signal and interference have overlap spectra. A number of publications have been published in adaptive filtering of biomedical signals, such as the ECG signal (1,7,14,16), evoked potentials (6), electromyographic signals (13), and electrogastrographic signals (2,3,4,6,12,15). Three kinds of adaptive filters have been proposed. These include time-, transform- and frequency-domain adaptive filters. It is known that the transform- and frequency-domain adaptive filters may have superior performance over the time-domain adaptive filter. However, in all of these previous biomedical applications adaptive filtering was performed in time domain. In this paper, all these three kinds of adaptive filters are explored, and their performances in adaptive cancellation of respiratory and motion artifacts are thoroughly investigated and compared with each other.

ADAPTIVE FILTERS

Time-Domain Adaptive Filter

The basic structure of a time-domain adaptive filter is illustrated in Fig. 1, where j stands for the time instant,

Acknowledgment—Acknowledgment is made to the Thomas F. and Kate Miller Jeffress Memorial Trust for the partial support of this research. The authors are also grateful to the reviewers for their constructive comments and suggestions.

Address correspondence to Jiande Chen, Ph.D., Box 145, Health Science Center, University of Virginia, Charlottesville, VA 22908.

(Received 25Jun93, Revised 6Jan94, Revised 28Mar94, Accepted 1Apr94)

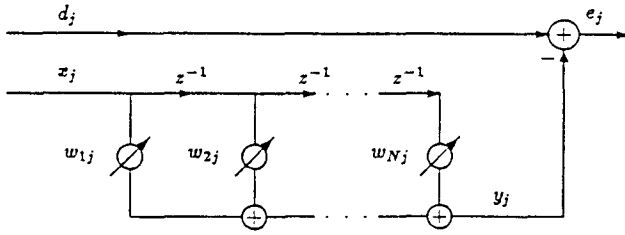


FIGURE 1. Time-domain adaptive filter.

z^{-1} for a unit delay, w_{kj} ($k = 1, 2, \dots, N$) are the weights of the adaptive filter and N is the order of the adaptive filter. The input to the adaptive filter is composed of a tapped delay line, $x_j, x_{j-1}, \dots, x_{j-N+1}$. The output of the adaptive filter at time j is denoted by y_j , which is the summed multiplication between the tap inputs and the filter weights:

$$y_j = \sum_{k=1}^N w_{kj} x_{j-k+1}. \quad (1)$$

The purpose of the adaptive filter can be described as:

Given a primary input signal d_j for an available input signal to the adaptive filter x_j , applying a certain criterion, produce an output that is an estimate of the primary input d_j in such a way that the residual error between d_j and the output of the adaptive filter y_j is made as small as possible in a statistical sense.

The residual error e_j in the figure can be written as

$$e_j = d_j - y_j. \quad (2)$$

Define

$$\mathbf{X}_j = [x_j, x_{j-1}, \dots, x_{j-N+1}]^T \quad (3)$$

as the filter input vector and

$$\mathbf{W}_j = [w_{1j}, w_{2j}, \dots, w_{Nj}]^T \quad (4)$$

as the filter weight vector, the filter output y_j is equal to the inner product of \mathbf{X}_j and \mathbf{W}_j ,

$$y_j = \mathbf{X}_j^T \mathbf{W}_j = \mathbf{W}_j^T \mathbf{X}_j. \quad (5)$$

The weights of the adaptive filter are adjusted for every input sample with the aim of minimizing the mean square error e_j . Assuming that reference input signal x_j and the primary input signal d_j are statistically stationary, a general expression for the mean square error as a function of the weight vector can be derived as follows:

$$e_j = d_j - y_j = d_j - \mathbf{X}_j^T \mathbf{W}_j \quad (6)$$

$$E[e_j^2] = E[d_j^2] - 2\mathbf{P}^T \mathbf{W}_j + \mathbf{W}_j^T \mathbf{R} \mathbf{W}_j,$$

where $E[\]$ stands for the expectation, \mathbf{P} is the cross-correlation vector defined by

$$\mathbf{P} = E[d_j X_j] \quad (7)$$

and R is the input auto-correlation matrix defined by

$$R = E[X_j X_j^T]. \quad (8)$$

Using the steepest-descent method and approximating gradient mean square error by gradient square error,

$$\begin{aligned} \mathbf{W}_{j+1} &= \mathbf{W}_j - \mu \nabla_j \\ \nabla_j &= \partial e_j^2 / \partial \mathbf{W}_j \end{aligned} \quad (9)$$

the famous least mean square error algorithm (16) can be derived:

$$\mathbf{W}_{j+1} = \mathbf{W}_j + 2\mu e_j \mathbf{X}_j, \quad (10)$$

where μ is the step-size that controls the stability, the rate of convergence, and the steady-state performance of the adaptive filter. Increase of the value of μ speeds up the convergence of the algorithm but increases the misadjustment in the steady state (16). In practical applications, the μ value is chosen as

$$0 < \mu \ll \frac{1}{\text{total input power}}. \quad (11)$$

Principle of Adaptive Noise Cancellation

Assume that the primary input d_j consists of a signal s_j and noise n_0 , and the reference input x_j consists of noise n_{1j} , and that noise n_{1j} is correlated with noise n_0 but not s_j , the minimization of the mean square error can be performed as follows (the time index j is omitted for simplicity):

$$e = s + n_0 - y \quad (12)$$

$$E[e^2] = E[s^2] + E[(n_0 - y)^2] + 2E[s(n_0 - y)].$$

Since signal s is uncorrelated with n_0 and with n_1 , we have

$$E[e^2] = E[s^2] + E[(n_0 - y)^2]. \quad (13)$$

From Eq. 13 we observe that the minimization of the mean square error can only result from the minimization of $E[(n_0 - y)^2]$, i.e.,

$$\min E[e^2] = E[s^2] + \min E[(n_0 - y)^2] \quad (14)$$

It can be seen from this equation that the smallest possible output power is $E[e^2] = E[s^2]$. This is achieved when the output of the adaptive filter y is a replica of the noise n_0 in the primary input.

Transform-Domain Adaptive Filter

It is known that the time-domain adaptive filter converges slowly, especially when the eigenvalue spread of the filter input autocorrelation matrix R is large (16). An

approach to accelerate the convergence rate is to somehow transform the input signal x_j into another signal with the corresponding autocorrelation matrix having small eigenvalue spread. This can be achieved by performing the adaptive filtering in some orthogonal domain. The structure of the transform domain adaptive filter is shown in Fig. 2. Define the input vector \mathbf{X}_j as,

$$\mathbf{X}_j = [x_j, x_{j-1}, \dots, x_{j-N+1}]^T \quad (15)$$

the orthogonal transform of the input vector, \mathbf{Z}_j as,

$$\mathbf{Z}_j = [z_j(0), z_j(1), \dots, z_j(N-1)]^T \quad (16)$$

and the filter weight vector, \mathbf{W}_j as,

$$\mathbf{W}_j = [w_j(0), w_j(1), \dots, w_j(N-1)]^T \quad (17)$$

the output of the adaptive filter y_j can be written as,

$$y_j = \mathbf{Z}_j^T \mathbf{W}_j. \quad (18)$$

The LMS algorithm for the adaptation of the filter weights is written as follows (13):

$$w_{j+1}(k) = w_j(k) + \frac{\mu}{\frac{1}{N} \sum_{k=0}^{N-1} |z_j(k)|^2} e_j z_j(k), \quad (19)$$

$$k = 0, 1, \dots, N-1,$$

where $w_j(k)$ is the k th filter weight at time instant j and μ is a small positive constant controlling the rate of convergence.

It is known that for a properly chosen orthogonal transform some reduction in the eigenvalue spread is expected. As a result, the transform-domain adaptive algorithm can be expected to have better convergence properties than the corresponding time-domain algorithm. In this paper, discrete cosine transform (DCT) is chosen for the orthogonal transform based on the following: (1) several studies have shown that the performance of the transform-domain adaptive filters using different transforms do not show noticeable differences (8,9,10); (2) unlike the discrete Fourier transform (DFT), the DCT does not involve complex arithmetic; (3) a faster recursive algorithm for the

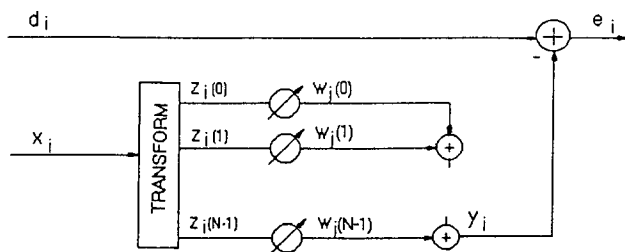


FIGURE 2. Transform-domain adaptive filter.

computation of the DCT was recently proposed by the authors (14). It requires only $2N$ (N is transform length) multiplications for each adaptation.

The running DCT of an input discrete series $x_j, x_{j-1}, \dots, x_{j-N+1}$ is defined as,

$$z_j(k) = \epsilon_k \sum_{m=0}^{N-1} x_{j-m} \cos \frac{(2m+1)k\pi}{2N}, \quad (20)$$

$$k = 0, 1, \dots, N-1.$$

Where,

$$\epsilon_j = \frac{\sqrt{2}}{N}, \quad k = 0 \quad (21)$$

$$\frac{2}{N}, \quad k = 1, 2, \dots, N-1$$

and N is the order of the adaptive filter. For a given j , $z_j(k)$ is the DCT in the variable k of the segment x_{j-m} of x_j . At the j th time instant, the data segment to be transformed is $x_j, x_{j-1}, \dots, x_{j-N+1}$, while at $(j+1)$ th time instant the segment to be transformed is $x_{j+1}, x_j, \dots, x_{j-N+2}$. Clearly, the data segment to be transformed is updated one sample at each new time instant.

Frequency-Domain Adaptive Filter

The frequency-domain adaptive filter is illustrated in Fig. 3. Fast Fourier transform is performed on both the primary input and the reference input. Define $X_k(m)$ and $D_k(m)$ as the k th frequency bin in the m th data block of the reference input and primary input, respectively. There are N complex weights $W_k(m)$, one corresponding to each frequency bin. The weighted filter outputs are given by

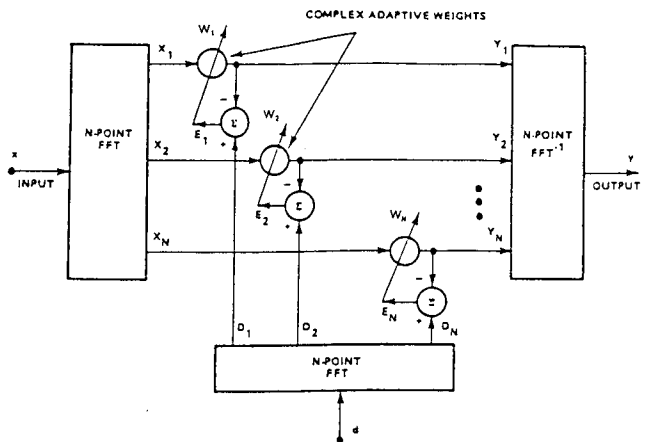


FIGURE 3. Frequency-domain adaptive filter.

$$Y_k(m) = W_k(m) X_k(m), k = 1, \dots, N \quad (22)$$

and are fed to an inverse FFT operator to produce N -point output signals. The weighted outputs are subtracted from the primary input transform values at corresponding frequencies to form N complex error signals:

$$e_k(m) = D_k(m) - Y_k(m), k = 1, \dots, N. \quad (23)$$

A fast convergence algorithm for the adaptation of the filter weights proposed in (11) is used in this paper and written as follows:

$$W_k(m+1) = \frac{\sum_{i=1}^m \lambda^{m-i} X_k^*(i) D_k(i)}{\lambda^m P_k^{-1}(0) + \sum_{i=1}^m \lambda^{m-i} X_k^*(i) X_k(i)}, \quad (24)$$

$$k = 1, \dots, N.$$

Where * indicates complex conjugate, $P_k^{-1}(0)$ and λ are constant values ($0 < \lambda < 1$) to be optimized for specific applications.

PERFORMANCE COMPARISON

Test Signals

A test signal d_j was produced for performance analysis of three different adaptive filters in the cancellation of motion artifacts in the EGG. In practice an EGG recording is composed of gastric electrical signal, respiratory and motion artifacts, and noise such as electrocardiogram. To simulate an EGG recording the test signal was generated by adding a pure electrical signal s_j of the stomach, a respiratory and motion signal r_j and Gaussian white noise n_j .

The pure gastric electrical signal s_j was obtained from a patient who underwent an abdominal surgery. A pair of electrodes was placed in the serosal surface of the stomach during surgery. The wires were brought out through the abdominal wall percutaneously and connected to a 5 channel amplifier (to be described in detail later). The respiratory and motion signal r_j was obtained from the same patient using a pneumotrace belt. The sampling frequency was 2 Hz. The pure gastric electric signal s_j obtained from the patient is presented in the top panel of Fig. 4. It has a frequency of 3.81 cycles/min (cpm) and peak amplitude of about 500 μ V. The second panel from the top shows the respiratory and motion artifacts r_j measured in the same patient using the pneumotrace belt. Panel C in Fig. 4 is the test signal d_j which is a combination of s_j , r_j , and Gaussian white noise n_j with a mean of 0 and a variance of 30.

For all experiments presented in this section, the primary input is the test signal: $d_j = s_j + r_j + n_j$. The reference input x_j is derived from the respiration and motion signal: $x_j = 0.5 r_j$. The misadjustment M_j is defined as the mean square error between the error signal e_j and the pure gastric signal s_j :

$$M_j = E[(e_j - s_j)^2].$$

Conventional Lowpass Filtering

Figure 5 presents the power spectra of the pure gastric signal and respiratory and motion artifacts. It can be seen that the gastric signal has a primary frequency of 3.81 cycles/min and a lot of harmonics. The respiratory and motion signal has a peak frequency around 15 cpm and high-power frequency components of 0–5 cpm. From this figure we can see clearly that the frequency of the gastric signal overlaps with that of the respiratory and motion artifacts. Conventional digital filtering is not adequate for the elimination of the respiratory and motion artifacts. Panel D in Fig. 4 shows the lowpass filtered (cutoff frequency: 6 cpm) version of the test signal d_j . Two main problems can be identified: (1) frequency components of the artifacts below 6 cpm cannot be eliminated; (2) while respiratory artifact (15 cpm) is substantially reduced, the waveform of the gastric signal is severely affected since the harmonics of the primary frequency of the gastric signal are filtered out.

Parameter Optimization of Adaptive Filters

In practical applications several parameters have to be specified for each kind of adaptive filters. The parameters for the time-domain and transform-domain adaptive filters are filter order N and step-size μ . A large μ results in fast convergence but large misadjustment in the steady state. The parameters for the frequency-domain adaptive filter are $P_k^{-1}(0)$, N , and λ . $P_k^{-1}(0)$ only affects the performance of the adaptive filter in initial state while λ controls the convergence of the adaptive filter. For a stationary input signal a large λ yields slow convergence and small misadjustment in the steady state. All these parameters must be optimized for each practical application.

A series of experiments were conducted using different filter orders ($N = 4, 8, 16, \text{ and } 32$) and different values of step-size ($\mu = 10^{-6}, 2 \times 10^{-7}, 10^{-7}, \text{ and } 10^{-8}$). It was found that: (1) a higher filter order resulted in faster convergence but larger misadjustment in the steady-state, whereas a lower filter order yielded slower convergence but smaller misadjustment in the steady-state (see Fig. 6); (2) a smaller μ resulted in slower convergence ($\mu = 10^{-8}$ was too small) while $\mu = 10^{-7}$ or 2×10^{-7} was a good choice which yielded fast convergence and small misadjustment (see Fig. 7). Similar tests were performed to investigate the effects of λ and $P_k^{-1}(0)$. In all experiments

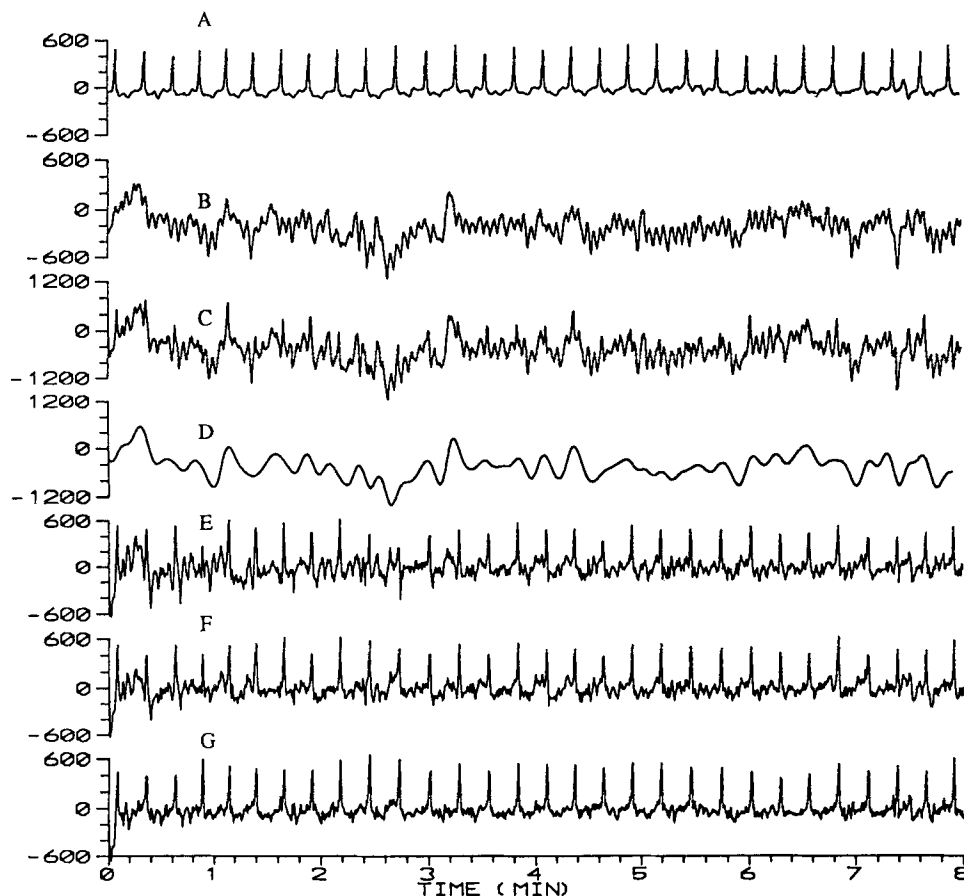


FIGURE 4. Simulated EGG signal (C) and its processed output (E–G). (A) Internally recorded gastric signal s_j from a patient. (B) Respiratory and motion artifacts r_j measured by a Pneumotrace belt. (C) Simulated surface EGG signal $d_j = s_j + r_j + n_j$ (n_j : Gaussian noise). (D) Simulated EGG after lowpass filtering (cutoff frequency = 6 cpm). (E–G) Simulated EGG after adaptive filtering in time-domain ($N = 8$, $\mu = 10^{-7}$) (E), transform-domain ($N = 8$, $\mu = 0.01$) (F), and frequency-domain ($N = 8$, $P_k^{-1}(0) = 1$ and $\lambda = 0.9$) (G), respectively.

presented in this paper the following values were used: $N = 8$, $\mu = 10^{-7}$ (time-domain), or 0.01 (transform-domain), $\lambda = 0.9$, and $P_k^{-1}(0) = 1$.

Comparison of Three Adaptive Filters

Performance. The misadjustment as a function of sample number with three different adaptive filters is presented in Fig. 8. It can be seen in this figure that frequency-domain adaptive filter has the best performance. It has a higher convergence speed and smaller misadjustments than the other two adaptive filters. The transform-domain adaptive filter has better performance than the time-domain adaptive filter.

The processed outputs of the test signal by the adaptive filters are presented in panels E–G of Fig. 4. It is seen that the artifacts are more effectively canceled using the frequency-domain adaptive filter (panel G) than the time-domain (panel E) and transform-domain (panel F) adaptive filters. This can be more clearly seen in Fig. 9A in which power spectra of the test signal d_j , the gastric signal

s_j and the processed output by frequency-domain adaptive filter are shown. The power spectrum of the processed output is almost the same as that the original gastric signal. The primary frequency component at 3.81 cpm is unchanged and all the harmonics are still present after adaptive filtering. The power spectra of the processed output by time- and transform-domain adaptive filters are presented in Fig. 9B. Carefully comparing these spectra we can see that the frequency-domain adaptive filter is of the best performance and the time-domain adaptive filter is of the worse performance.

Computational Complexity. The multiplications required for processing N samples for different adaptive filters are listed as follows:

time-domain adaptive filter: $2N^2$ (N adaptations)

transform-domain adaptive filter: $N^2 + 2N^2$ (N adaptations)

frequency-domain adaptive filter: $3\{N/2(\log_2 N)\} + 2N$ (one adaptation).

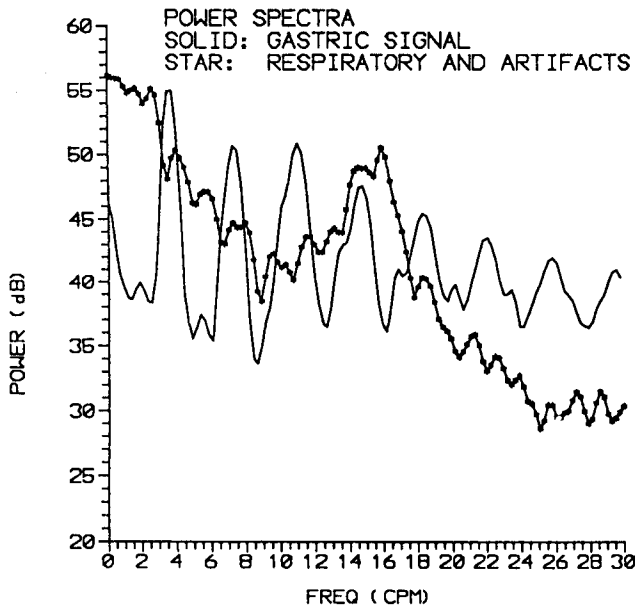


FIGURE 5. Power spectra of the gastric signal s_g (solid curve) and respiratory and motion artifacts (star curve). The gastric signal has a primary frequency of 3.81 cpm and harmonics. The signal and artifacts have overlap frequencies.

For $N = 8$, the multiplications required for time-, transform-, and frequency-domain adaptive filters are 128, 192, and 52, respectively. Thus, the frequency-domain adaptive filter is the simplest in computational complexity for filter order of 8. The larger the filter order N , the more the computational savings are attained with the frequency-domain adaptive filter.

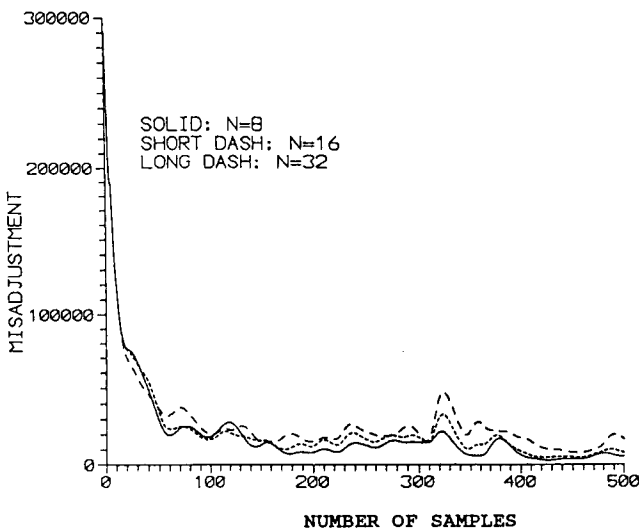


FIGURE 6. Effect of filter order on time-domain adaptive filtering. A higher filter order resulted in faster convergence but a larger misadjustment in the steady-state, whereas a lower filter order yielded slower convergence but a smaller misadjustment in the steady-state.

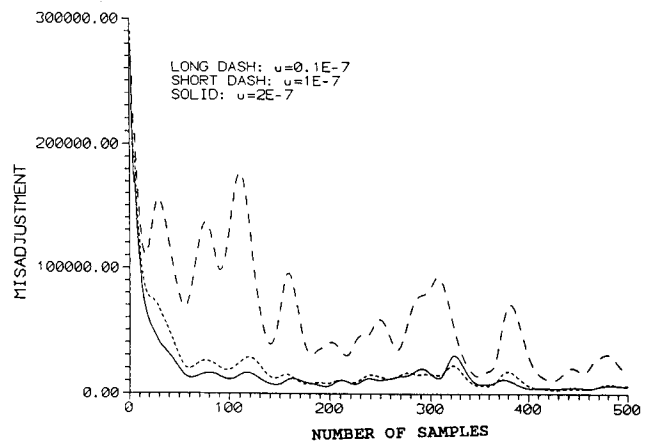


FIGURE 7. Effect of step size on time-domain adaptive filtering. A smaller μ resulted in slow convergence ($\mu = 10^{-8}$ was too small) while $\mu = 10^{-7}$ or 2×10^{-7} was a good choice which yielded fast convergence and small misadjustment.

CANCELLATION OF RESPIRATORY AND MOTION ARTIFACTS

Measurement of the EGG

The EGG was measured in five healthy volunteers by placing two silver-silver chloride electrodes on the abdominal skin over the stomach. The impedance between the bipolar electrodes was reduced to below 10 k Ω by lightly abrading skin using sandy skin-prep gel. The bipolar electrical signal was amplified with a frequency range of 0.016–0.3 Hz, on-line digitized (8 channel, 12-bit A/D converter; Keithley Metrabyte, MA, U.S.A.) with a sampling frequency of 2 Hz, displayed and stored on a

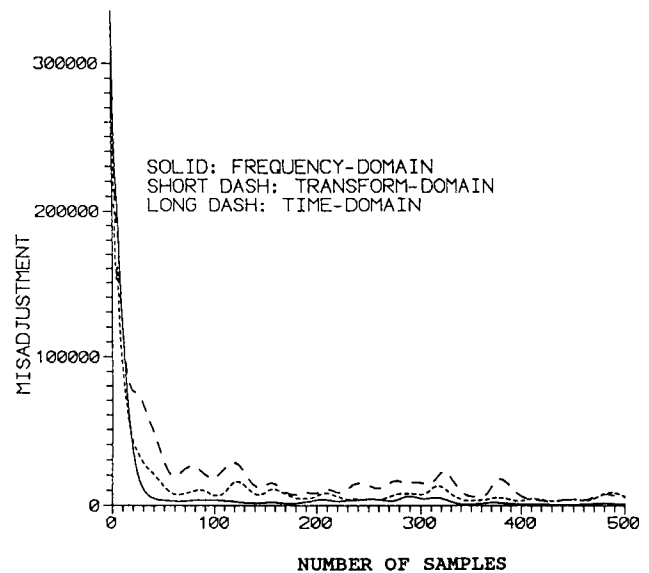


FIGURE 8. Comparison of time- ($N = 8, \mu = 10^{-7}$), transform- ($N = 8, \mu = 0.01$), and frequency-domain ($N = 8, P_k^{-1}(0) = 1$ and $\lambda = 0.9$) adaptive filters.

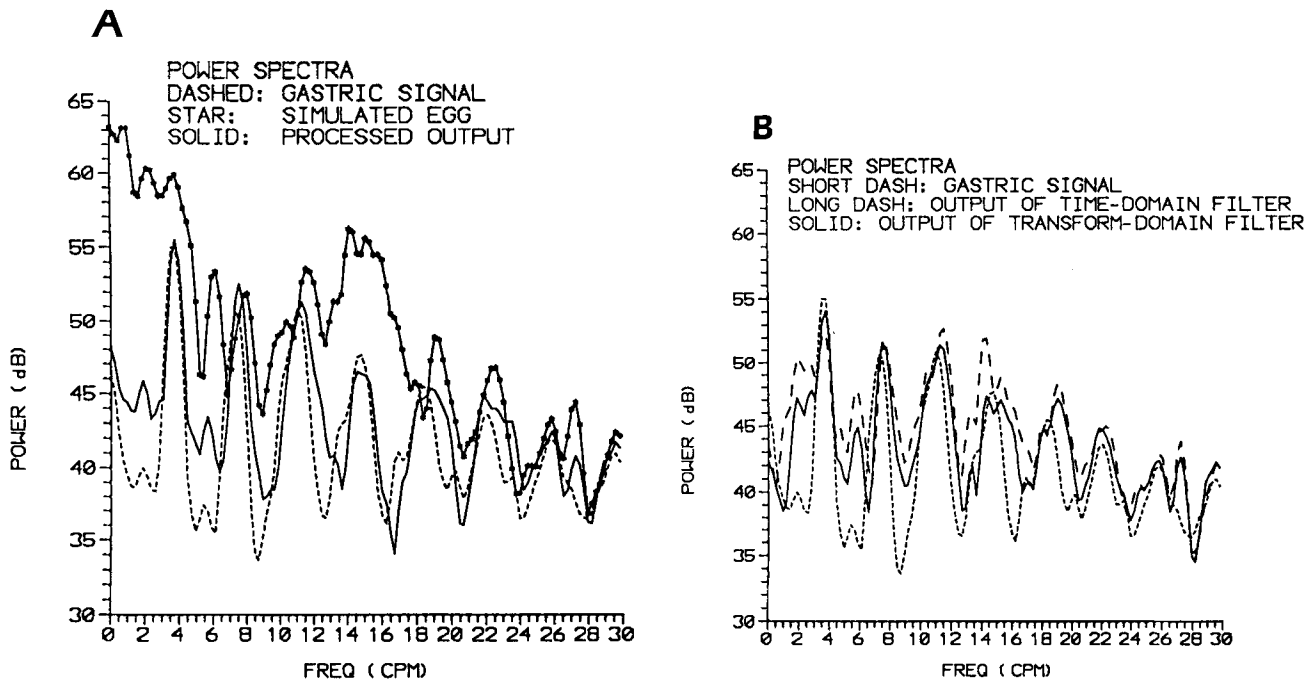


FIGURE 9. (A) Power spectra of the simulated EGG (star), the gastric signal (dash) and the processed output after frequency-domain adaptive filtering (solid, $N = 8$, $P_k^{-1}(0) = 1$ and $\lambda = 0.9$). (B) Power spectra of the gastric signal (short dash), and processed outputs after time-domain adaptive filtering (long dash, $N = 8$, $\mu = 10^{-7}$) and transform-domain adaptive filtering (solid, $N = 8$, $\mu = 0.01$).

personal computer using CODAS software (Keithley Metrabyte, MA, U.S.A.). The amplifier has four channels for the EGG and one channel for respiration (Sandhill, CO, U.S.A.). Respiration was simultaneously recorded using a Pneumotrace belt, digitized and stored in the same way as for the EGG signal.

Cancellation of Respiratory and Motion Artifacts

A typical EGG recording obtained in one of the five healthy volunteers is presented in Fig. 10 (top panel). The slow activity with a frequency of about 2.5 cpm is the gastric slow wave. The fast activities superimposed on the gastric slow waves are mainly respiratory artifacts. The bottom panel shows the EGG after frequency-domain adaptive filtering. It can be seen that the respiratory arti-

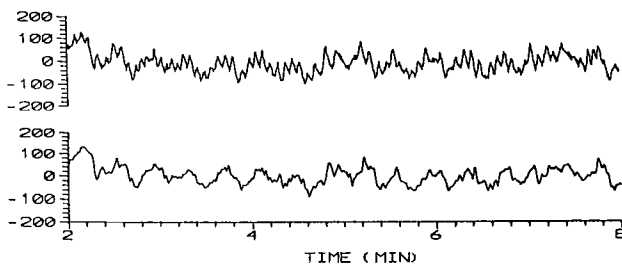


FIGURE 10. An EGG recording (top panel) obtained in one of the five healthy volunteers and the processed EGG by frequency-domain adaptive filter ($N = 8$, $P_k^{-1}(0) = 1$ and $\lambda = 0.9$).

facts are substantially reduced. The power spectra of the EGG recording before (solid curve) and after (dash curve) adaptive filtering are presented in Fig. 11. The peak power at 2.5 cpm is attributed to the gastric slow wave, whereas frequency components around 12 cpm show respiratory artifacts. From this figure we can see that about 10 dB cancellation of respiratory artifact is achieved while the

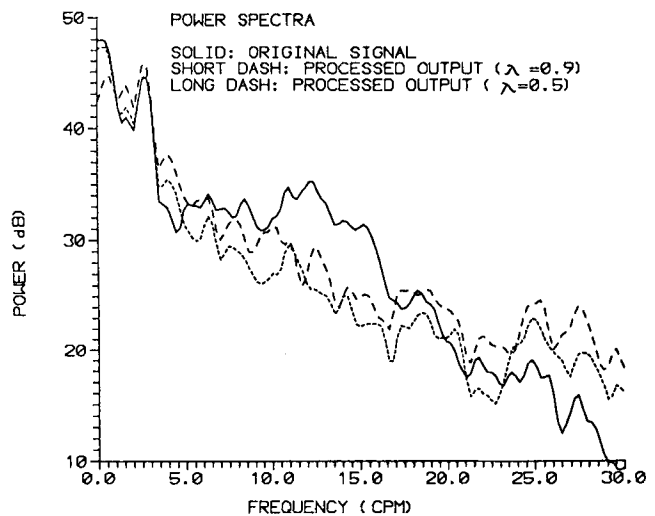


FIGURE 11. Power spectra of the original EGG (solid curve) and processed outputs by frequency-domain adaptive filter with $\lambda = 0.9$ (short dash) and $\lambda = 0.5$ (long dash).

gastric signal is not affected after adaptive filtering with $\lambda = 0.9$ (short dash curve). The increased power around 25 cpm is attributed to misadjustment of the adaptive filter. It can also be seen from this figure that a small λ (0.5) results in less cancellation of respiratory artifacts and larger misadjustment.

The time- and transform-domain adaptive filters have also been applied for the cancellation of the respiratory artifact in the EGG and compared with the frequency-domain adaptive filter. The results were the same as those obtained from the simulations, *i.e.*, the frequency-domain adaptive filter attains better performance than the time- and transform-domain adaptive filters in the cancellation of the respiratory artifact.

For cancellation of nonstationary motion artifacts, however, the time-domain adaptive filter yields better performance than the frequency-domain adaptive filter. A typical result showing the cancellation of nonstationary motion artifact using the time-domain adaptive filter is presented in Fig. 12. Panel A shows about 1 min EGG recording with severe motion artifact attributed to deep breath. Panel B is the reference signal recorded by the Pneumotrace belt. The bottom panel (E) shows the EGG after adaptive filtering in time-domain. The normalized least mean square algorithm was applied to avoid divergence and a large step-size [$\mu = 0.5/X_j^T X_j$] was used in order to follow time-varying characteristic of the input signal. It is seen that the severe motion artifacts are effectively removed. In comparison with the time-domain adaptive filter, the frequency-domain and transform-domain adaptive filters did not provide satisfactory results as shown in (C) and (D), respectively.

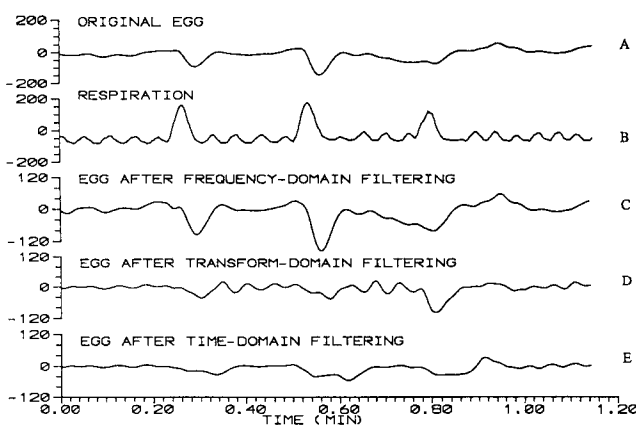


FIGURE 12. Adaptive cancellation of nonstationary motion artifacts. (A) An EGG recording with severe motion artifacts due to deep breath of the subject. (B) Recorded respiration by a Pneumotrace belt. Three high peaks in the recording were attributed to deep breath. (C–E) EGG after adaptive filtering in frequency-domain (C), transform-domain (D), and time-domain (E), respectively.

DISCUSSION AND CONCLUSIONS

The time-, transform-, and frequency-domain adaptive filters are presented and their performances in the cancellation of respiratory and motion artifacts in the EGG are investigated and compared.

To investigate the performance (misadjustment) of the adaptive filter a simulated test signal is needed. It is a common practice to use a computer-generated artificial test signal to simulate the real-world signal. In this paper, however we used the internal gastric electrical signal as the “pure” gastric signal. It is believed that the use of internal gastric electrical signal is better than otherwise a computer-generated “artificial” signal based on the following. (1) Previous studies (5,12) have shown that the frequency of the surface gastric electrical recording is the same as that of the internal signal. Therefore the use of the internal signal as the test signal reflects the frequency of the surface recording as well as its time-varying characteristics. (2) Although the waveform of the internal signal is not the same as the surface signal, it is more difficult to restore it from the test signal because the internal signal contains more harmonics than the surface signal. That is, the test signal used in this paper is more difficult to process than the actual surface signal. (3) The signal-to-noise ratio (SNR) of the test signal used in this paper is much lower than the actual surface signal.

Both simulation results and real EGG applications have shown that the frequency-domain adaptive filter has superior performance over the other two adaptive filters in the cancellation of stationary noise, such as stationary respiratory artifacts. The frequency-domain adaptive filter has faster convergence and smaller misadjustment than the time- and transform-domain adaptive filters. A frequency-domain adaptive filter with a length of N can be considered as N adaptive filters each with a single weight. Each filter weight is optimized during the adaptation based on the characteristic of the corresponding frequency bin and thus resulting in better performance. The transform-domain adaptive filter produces faster convergence than the time-domain adaptive filter for adaptive filtering of input signals with a larger eigenvalue spread. This is because the orthogonal transform reduces the eigenvalue spread of the input autocorrelation matrix. The frequency-domain adaptive signal has lowest computational complexity as well.

For the cancellation of nonstationary motion artifact as shown in Fig. 12, however, the time-domain adaptive filter provides better performance than the frequency-domain adaptive filter. This is because the time-domain adaptive filter adjusts filter weights once for each incoming data sample while the frequency-domain adaptive filter processes data in a block manner: filter weights are

adapted only once for every N incoming data samples. For a stationary input, the signal characteristic of the first N samples is similar to that of the next N samples and the filter weights can be adjusted to their optimal values. After a certain number of adaptations the filter weights reach their optimal values. For a nonstationary input, however, the signal characteristic is time-varying. The signal characteristic of the first N samples may be quite different from that of the next N samples and the filter weights may never reach their optimal values which are also time-varying. Therefore, the frequency-domain adaptive filter is not well suited for processing nonstationary signals with rapid characteristic changes.

REFERENCES

1. Akkiraju, P.; Reddy, D.C. Adaptive cancellation technique in processing myoelectric activity of respiratory muscles. *IEEE Trans. Biomed. Eng. BME* 39:652-655; 1992.
2. Chen, J.; Vandewalle, J.; Vantrappen, G.; Janssens, J. Adaptive spectral analysis of cutaneous electrogastric signal using autoregressive moving average modelling. *Med. Biol. Eng. Comput.* 28:531-536; 1990.
3. Chen, J.; Vandewalle, J.; Vantrappen, G.; Janssens, J. Adaptive method for cancellation of respiratory artifact in electrogastric measurements. *Med. Biol. Eng. Comput.* 27:57-63; 1989.
4. Chen, J.; Vandewalle, J.; Vantrappen, G.; Janssens, J. Multichannel adaptive enhancement of the electrogastrogram. *IEEE Trans. Biomed. Eng. BME* 37:285-294; 1991.
5. Chen, J.; McCallum, R.W. Electrogastrography: measurement, analysis and prospective applications. *Med. Biol. Eng. Comput.* 29:339-350; 1991.
6. Chen, J.; Stewart, W.R.; McCallum, R.W. Spectral analysis of episodic rhythmic variations in myoelectric signal of the stomach. *IEEE Trans. Biomed. Eng. BME* 40:128-135; 1993.
7. Ferrara, E.R.; Widrow, B. Fetal electrocardiogram enhancement by time-sequenced adaptive filtering. *IEEE Trans. Biomed. Eng. BME* 29:458-460; 1982.
8. Lee, J.C.; Un, C.K. Performance of transform-domain LMS adaptive digital filter. *IEEE Trans. Acoust. Speech Sig. Proc.* 34:499-501; 1986.
9. Lin, Z.Y.; Chen, J.D.Z. Transform domain adaptive filtering using recursive DCT and its application in surface recording of small intestine. *Med. Biol. Eng. Comput.* In press.
10. Narayan, S.S.; Peterson, A.M.; Narasimha, M.J. Transform domain LMS algorithm. *IEEE Trans. Acoust. Speech Sig. Proc.* 31:609-614; 1983.
11. Ogue, J.C.; Saito, T.; Hoshiko, Y. A fast convergence frequency domain adaptive filter. *IEEE Trans. Acoust. Speech Sig. Proc.* 31:1312-1314; 1983.
12. Smout, A.J.P.M.; Van der Schee, E.J.; Grashuis, J.L. What is measured in electrogastrography? *Dig. Dis. Sci.* 25:179-187; 1980.
13. Thakor, N.V. Adaptive filtering of evoked potentials. *IEEE Trans. Biomed. Eng. BME* 34:6-12; 1987.
14. Thakor, N.V.; Zhu, Y.Z. Application of adaptive filtering to ECG analysis: noise cancellation and arrhythmia detection. *IEEE Trans. Biomed. Eng. BME* 38:785-794; 1991.
15. Van der Schee, E.J.; Kentie, M.A.; Grashuis, L.J.; Smout, A.J.P.M. Adaptive filtering of canine electrogastrographic signals. Part 1: System design. *Med. Biol. Eng. Comput.* 19:759-764; 1981.
16. Widrow, B.; Glover, J.R.; McCool, J.M.; *et al.* Adaptive noise canceling: principles and applications. *Proc. IEEE.* 63:1692-1716; 1975.